J. Fluid Mech. (1984), *vol.* 144, *pp.* 445–462
Printed in Great Britain

Two-dimensional impervious sails: experimental results compared with theory

By B. G. NEWMAN AND H. T. LOW†
Department of Mechanical Engineering, McGill University, Montreal

(Received 15 December 1982 and in revised form 9 September 1983)

Experiments have been made on quasi two-dimensional sails of small camber and at small incidence. Four excess-length ratios have been tested at a Reynolds number of 1.2×10^5. The results for lift, tension, centre of lift, maximum camber and its position, and leading- and trailing-edge membrane angles have been compared with existing inviscid theories and show poor agreement in general. This is attributed to leading- and trailing-edge flow separations as indicated by supplementary flow-visualization experiments. The optimum incidences in particular are much greater than the theoretical value of 0°. Luffing occurs at slightly negative incidences and appears to be a dynamic instability. The highest lift-to-drag ratio obtained was 16.5 on a membrane with an excess-length ratio of 0.03.

1. Introduction

The purpose of this paper is to present measurements on quasi two-dimensional impervious sails of small camber and at low angles of attack, and to compare these experimental results with available inviscid theories. The significance of the work to the design of real sails is debatable. Milgram (1971, 1972) takes the view that by suitable cut and allowance for stretch any desired shape of sail is possible in three dimensions. However, jibs and foresails are relatively unconstrained and are very nearly developable surfaces. Thus changes of sail shape with wind strength may occur which are similar to those observed in two dimensions. Certainly the study of luffing in two dimensions throws light on the behaviour of real sails at low angles of attack (Marchaj 1979).

The flow past two-dimensional planar sails was first analysed using thin-aerofoil theory assuming small incidence and camber in irrotational inviscid flow by Voelz (1950), Thwaites (1961) and Nielsen (1963). A significant feature of these analyses was that the sail or membrane tension coefficient C_T and the normalized lift coefficient slope C_L/α were unique functions of a combination of the two non-dimensional parameters: the excess-length ratio $\epsilon = (l-c)/c$, where l is the length of the membrane and c is the distance between the leading-edge and trailing edge, or between luff and leech; and the angle of incidence α.

The combination is $\alpha/\epsilon^{\frac{1}{2}}$. The shape when normalized as $y/c\alpha$ against x/c is also uniquely determined by the same combined parameter (Newman 1982).

Numerical solutions were obtained by solving the basic integral equation of the analysis using an appropriate series expansion for the slope of the membrane. As expected there is predicted to be a suction force acting on the leading edge. This force

† Permanent address: Department of Mechanical and Production Engineering, National University of Singapore.

is only zero at 0° incidence, which is the 'ideal' incidence at which the flow attaches smoothly at the leading edge (Robinson & Laurmann 1956; Thwaites 1960) and the Kutta condition is satisfied at both the leading and trailing edges.

Vanden-Broeck (1982) has extended the analysis by removing the restrictions of small camber and incidence. The problem is then nonlinear and C_T is no longer a function of $\alpha/\epsilon^{\frac{1}{2}}$ only. Linear theory has been extended to account for sail porosity (Barakat 1968) and sail stretch (Ormiston 1971). Murai & Maruyama (1980, 1982) have analysed the Princeton sail aerofoil, which uses a double membrane wrapped round a cylindrical leading edge.

Very few measurements have been made on single-membrane sail aerofoils. Thwaites (1961) compared sail shape with one set of experimental measurements made by Tanner. Nielsen (1963) summarized some results made in a small wind tunnel at a Reynolds number of about 7×10^5. Although no details were given, it was reported that the lift increment due to camber was one-third to one-half the theoretical value. The lift curve slope was nonlinear for cambers exceeding 15% ($\epsilon > 0.06$) and had an average value greater than the theory. For $\epsilon < 0.06$ the lift-curve slope, although not the lift itself, agreed with theory. The centre of lift was in good agreement with theory for cambers less than 15%. Chapleo (1968) gives some numerical values for lift and drag coefficients which were measured by undergraduate students at Southampton University. He pointed out that the values of ϵ for each set of results is uncertain by as much as 100% because of deflection of the supports and other experimental difficulties.

Measurements of lift and drag have been made on double membrane aerofoils by Robert & Newman (1979), but again the effective camber is uncertain.

Clearly there are too few data with which to realistically assess the classical single-membrane aerofoil theories. In particular the tension T in the membrane has not been measured. Experiments are difficult because any aerodynamic interference of the leading edge or luff support should be small, while, at the same time, the support must not sag so much that it alters ϵ in the spanwise direction and thus affects the two-dimensional nature of the test.

In the present paper experiments have been made on low-aspect-ratio models of chord 78 mm and span 152 mm mounted vertically between walls to which boundary-layer suction was applied ahead of the models. The sidewalls were left open to the atmosphere to reduce wind-tunnel interference. The Reynolds number for the bulk of the tests was 1.2×10^5 with some supporting measurements at 0.7×10^5. The forces at each end of the luff and leech supports were measured and interpreted to give lift, drag, moment, centre of lift, tension and membrane angles at luff and leech. Flow visualization was used on the main models and on other models in a smoke tunnel ($Re \approx 10^4$) in order to determine the reasons for the discrepancies between experiment and theory. Some photographs of membrane shape were also taken to determine the maximum camber and its position.

2. Theoretical considerations

2.1. *Outline of linear theory*

The steady flow past two-dimensional planar sails (figure 1) has been analysed for small incidence and camber in irrotational inviscid flow by Voelz (1950), Thwaites (1961) and Nielsen (1963). In real flow the membrane tension decreases slightly from leading to trailing edge owing to skin friction. In inviscid flow the tension is constant.

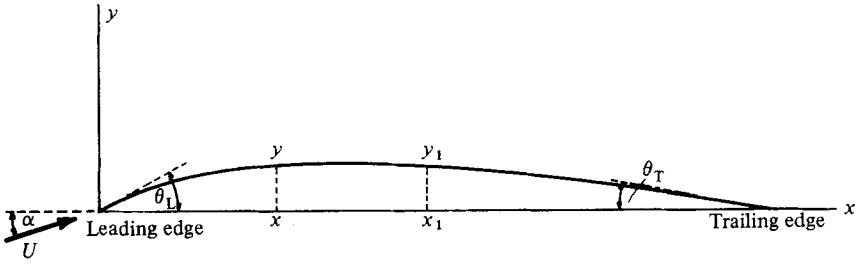

FIGURE 1. Inviscid flow past a two-dimensional sail.

The aerofoil chord is taken as unity. On this scale the length of the sail is l. The pressure difference across the sail at point $x = x_1$ is

$$\Delta p = -T\frac{\mathrm{d}^2 y_1}{\mathrm{d}x_1^2} \tag{1}$$

because the slope is small and the tension T is constant. Δp also equals $\rho U k_1$, a result which comes from either Bernoulli's equation for top and bottom streamlines, or the Kutta–Joukowski condition. k_1 is the local strength per unit length of the vortex sheet which represents the sail. $k_1 \ll U$ due to the assumptions of thin aerofoil theory.

At any other point x on the sail, the flow due to the net effect of the vortex sheet and the oncoming flow must be locally parallel to the sail in figure 1. Thus

$$\alpha + \frac{1}{U}\int_0^1 \frac{k_1\,\mathrm{d}x_1}{2\pi(x_1 - x)} = \frac{\mathrm{d}y}{\mathrm{d}x},$$

or, substituting for k_1 from (1) and rearranging (Newman 1982),

$$1 - \frac{T}{\rho U^2}\int_0^1 \frac{\dfrac{\mathrm{d}^2(y_1/\alpha)}{\mathrm{d}x_1^2}}{2\pi(x_1 - x)}\mathrm{d}x_1 = \frac{\mathrm{d}(y/\alpha)}{\mathrm{d}x}, \tag{2}$$

which shows that

$$\frac{y}{\alpha} = f(x, C_T), \tag{3}$$

where the tension coefficient $C_T = T/\frac{1}{2}\rho U^2 l$. The length of the membrane

$$l = \int_0^1 \left(1 + \frac{1}{2}\left(\frac{\mathrm{d}y}{\mathrm{d}x}\right)^2\right)\mathrm{d}x, \quad l - 1 = \frac{\alpha^2}{2}\int_0^1 \left[\frac{\mathrm{d}(y/\alpha)}{\mathrm{d}x}\right]^2 \mathrm{d}x = \alpha^2\,\text{function}\,(C_T).$$

Thus

$$C_T = \text{function}\,(\alpha(l-1)^{-\frac{1}{2}}) = \text{function}\,(\alpha\epsilon^{-\frac{1}{2}}), \tag{4}$$

where ϵ is the excess-length ratio $(l-1)/1$, or $(l-c)/c$ if the chord c is not unity. The total lift

$$L = \int_0^1 \Delta p\,\mathrm{d}x = -T\alpha\int_0^1 \frac{\mathrm{d}^2(y/\alpha)}{\mathrm{d}x^2}\mathrm{d}x.$$

Thus

$$\frac{C_L}{\alpha} = \text{function}\,(C_T) = \text{function}\,(\alpha\epsilon^{-\frac{1}{2}}). \tag{5}$$

Similarly it may be shown that θ_L/α, θ_T/α, x_{CL}, max. camber/$\epsilon^{\frac{1}{2}}$ and its position are all functions of C_T or alternatively, $\alpha\epsilon^{-\frac{1}{2}}$. In the above, θ_L and θ_T are the small membrane angles at the leading and trailing edges. x_{CL} identifies the centre of lift.

FIGURE 2. Kutta condition satisfied at the leading edge but not the trailing edge.

Nielsen (1963) solved (2) to obtain these relationships by expressing the pressure difference as a suitable Fourier series with a lead term representing the infinite suction on the leading edge which exists at other than ideal incidences. The Kutta condition was used at the trailing edge.

For a rigid aerofoil there is only one optimum incidence, but for a sail there are several. The first occurs at $\alpha = 0$ for $C_T = 1.727$ and the second at $\alpha\epsilon^{-\frac{1}{2}} = -0.6$ for $C_T = 0.726$. In the range $0.726 < C_T < 1.727$ the membrane is S-shaped having one point of inflection. For $C_T > 1.727$ the sail has a more conventional shape with curvature of one sign only and is concave to the oncoming flow.

2.2. *Modified linear theory*

In interpreting the experiments that will be described later, it is interesting to consider solutions of the sail equation (2) for which the Kutta condition is satisfied at the leading edge but not at the trailing edge and for which the circulation is less than that which would satisfy the Kutta condition at the trailing edge. The situation is as shown in figure 2.

For positive incidences the rear stagnation point is now on the upper or leeward side of the sail, and thus the curvature of the sail changes sign near the trailing edge as shown. If the flow is thought of as reversed, it is seen that the previous solutions for $0.726 < C_T < 1.727$ apply. Thus there is a second set of solutions which may also be stated in terms of the collapsed parameter $\alpha/\epsilon^{\frac{1}{2}}$. They are taken to be valid near the experimentally determined ideal incidence for cases when the conventional trailing-edge Kutta condition might not apply. Nielsen (1963) presents tabulated results only for $C_T > 1.727$. His numerical method has therefore been programmed and results obtained for values of C_T down to 0.726. They are consistent with those presented graphically by Thwaites (1961).

2.3. *Simple second-order results*

Certain results may be obtained by very simple considerations from figure 3. Assume that the suction force makes only a small angle β with the chord. This seems reasonable since the other angles α, θ_L and θ_T are also small. Moreover β is zero for linear theory (Thwaites 1960). The forces T and S at the leading-edge and T at the trailing-edge combine to produce the lift L. The drag is zero within the assumption of inviscid flow.

Resolving parallel to U

$$S[1-\tfrac{1}{2}(\beta-\alpha)^2] = \tfrac{1}{2}T[(\theta_T+\alpha)^2-(\theta_L-\alpha)^2].$$

Thus

$$C_S = \tfrac{1}{2}C_T(\theta_T+\theta_L)(\theta_T-\theta_L+2\alpha). \tag{6}$$

$C_T = O(1)$, and hence $C_S = O(\theta^2)$. This is consistent with the value for a circular-arc aerofoil (Robinson & Laurmann 1956).

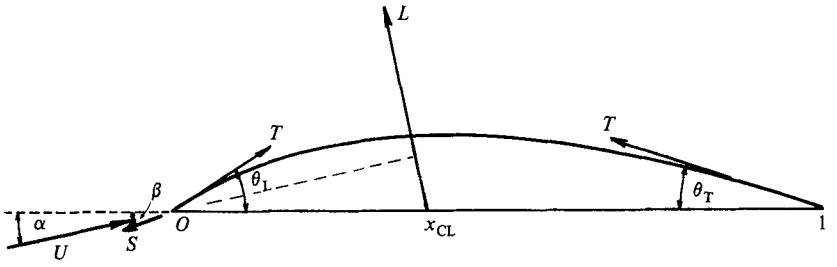

FIGURE 3. Force components for inviscid flow.

Resolving perpendicular to U,

$$T(\theta_L+\theta_T) - S(\beta-\alpha) = L.$$

Thus

$$C_L = C_T(\theta_L+\theta_T) \quad \text{correct to } O(\theta^2).$$

To be consistent with the complete analysis, this would be written

$$\frac{C_L}{\alpha} = C_T\left(\frac{\theta_L}{\alpha}+\frac{\theta_T}{\alpha}\right). \tag{7}$$

Taking moments about the leading edge,

$$x_{CL}\, L\cos\alpha = T\sin\theta_T,$$

$$x_{CL} = \frac{\theta_T}{\theta_L+\theta_T} = \frac{\theta_T/\alpha}{\theta_L/\alpha+\theta_T/\alpha} \quad \text{correct to } O(\theta^2). \tag{8}$$

These results are compatible with the values tabulated by Nielsen (1963). Jackson (1983) has recently used a similar approach in developing an approximate method for solving the sail equation (2).

From (6) and (7)

$$\frac{C_S}{C_L} = \tfrac{1}{2}(\theta_T-\theta_L+2\alpha). \tag{9}$$

In a real viscous flow the suction force S is absent owing to leading-edge separation, and thus there is an additional profile drag of magnitude S. Equation (9) may therefore be expected to give the minimum drag-to-lift ratio in practice.

3. Experiment

3.1. *Experimental arrangement*

The leading and trailing edges of the membrane models were mounted on vertical strips, which were chosen to be small compared with the chord of the model to avoid aerodynamic interference while at the same time not so small that the deflection of these supports would incur a significant variation of ϵ along the span.

The experiments were conducted in a new working section connected via an extra contraction to the 762 mm × 432 mm Blower Cascade Wind Tunnel in the McGill Aerodynamics Laboratory (Wygnanski & Gartshore 1963). At the exit of the unmodified wind tunnel, when being driven by the 25 h.p. a.c. motor, the turbulence intensity is 1.3% at low velocities and decreases to 0.3% at high velocities. These turbulence levels will be significantly reduced by the extra 17:6 contraction. The

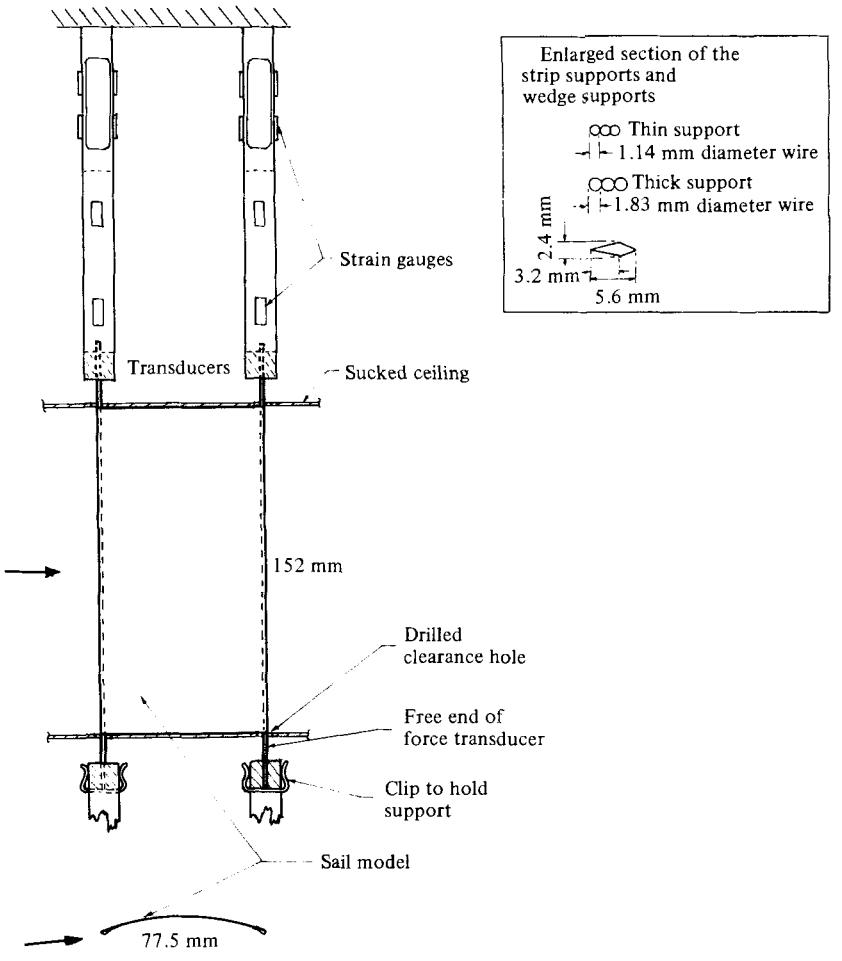

FIGURE 4. Sail model, supports and force transducers.

width of the new working section was 762 mm, and, to reduce tunnel interference effects, the sides were left open to the laboratory. The boundary layers on the floor and ceiling of the working section were sucked away through suction surfaces extending 420 mm in front of the model. The typical average suction velocities were 0.03 of the tunnel velocity, and the boundary-layer thickness, which was 15 mm without suction, was reduced to 1.5 mm.

For force measurements each end of the supports was attached to a two-component force transducer (figure 4). The force transducers were each mounted on a cylindrical housing, which could be rotated to change the overall incidence of the sail model. Provision was made for accurately aligning the transducers. Each two-component transducer consisted of a pair of parallel flexures stacked one above the other, with their flexible directions perpendicular to each other. The strain on each set of parallel flexures was measured by four strain gauges, which were glued to the flexures and connected to form a conventional Wheatstone bridge. The length of each pair of flexures was such that one was about twice as sensitive as the other, the pair in the direction of the sail chord being the stiffer to reduce variation of sail chord under load. The sensitivity of this flexure was better than ± 0.01 N.

The leading and trailing-edge strip supports each consisted of three steel wires soldered together as shown in figure 4. The outer wire was extended through holes in the floor and ceiling of the tunnel and was mounted in holes at the end of each force transducer. The wires could rotate freely and the tension in them was sensibly zero. Direct calibration confirmed that the transducers attached to each support collectively measured the net horizontal force on the support irrespective of where it acted.

The sail models were made of impervious Stablekote II ripstop nylon, a light, closely woven cloth used for spinnaker sails with a mass of 38 g/m^2.

The chord and span of each model were respectively 77.5 and 154 mm. The latter dimension was made slightly larger than the 152 mm height of the working section so as to reduce flow leakage. Initially models with $\epsilon = 0.03$, 0.05 and 0.10 were tested, and these were folded round supports to form a seam which was either glued or stitched. The values of ϵ were obtained by measuring the membrane length and are estimated to be accurate to ± 0.004. The stretch of the cloth was estimated to increase ϵ by less than 0.001 for the range of tunnel speeds that were used. The sail profiles were recorded photographically and the maximum camber and its position were measured.

On completion of the main tests it appeared desirable to test a smaller value of ϵ, and this proved to be difficult because of the high sail tension. New supports (figure 4) were made, consisting of small pivoted wedges 5.6 mm long in the sail-chord direction and of width 2.4 mm. The membrane was difficult to make and also difficult to measure. ϵ was estimated from the measured maximum camber using Nielsen's (1963) tabulated values. Under load at 6° incidence the model had $\epsilon = 0.015$ at both ends and $\epsilon = 0.017$ in the middle of the span. This midspan value was observed to extend over a large portion of the span and is therefore quoted for this membrane.

3.2. *Checks on the apparatus*

The tunnel-interference effects on the streamlined membrane was estimated from the formulae for an open-jet tunnel given in Pankhurst & Holder (1952). All corrections were found to be negligible.

Some measurements were made on the model with $\epsilon = 0.03$ using supports that were 1.6 times larger than those of the main experiments (figure 4). This was done to assess the effect of support size. The changes were minor (figures 5–10) except for one or two values at large α. It was therefore concluded that the present results are effectively insensitive to support size and may usefully be compared with the sail theories.

4. Experimental results and comparison with theory

The experimental results for normalized lift, tension, centre of pressure, leading- and trailing-edge membrane angles, camber ratio and position of maximum camber are shown in figures 5–10, where they are plotted against the theoretical parameter $\alpha/\epsilon^{\frac{1}{2}}$. C_L and the membrane angles are normalized using α, and the camber ratio by using $\epsilon^{\frac{1}{2}}$; both are presented in this way by Nielsen (1963).

It is seen that the results do *not* collapse onto a single curve independent of ϵ in each case. This is particularly so for lift, tension and, to a lesser extent, the centre of lift. The results for small camber, $\epsilon = 0.017$ and 0.03, exhibit the same trends as the theory, but the degree of agreement is far from satisfactory. A notable feature of the lift curve (figure 5) is that, for $\epsilon > 0.03$, α/C_L increases with increasing camber,

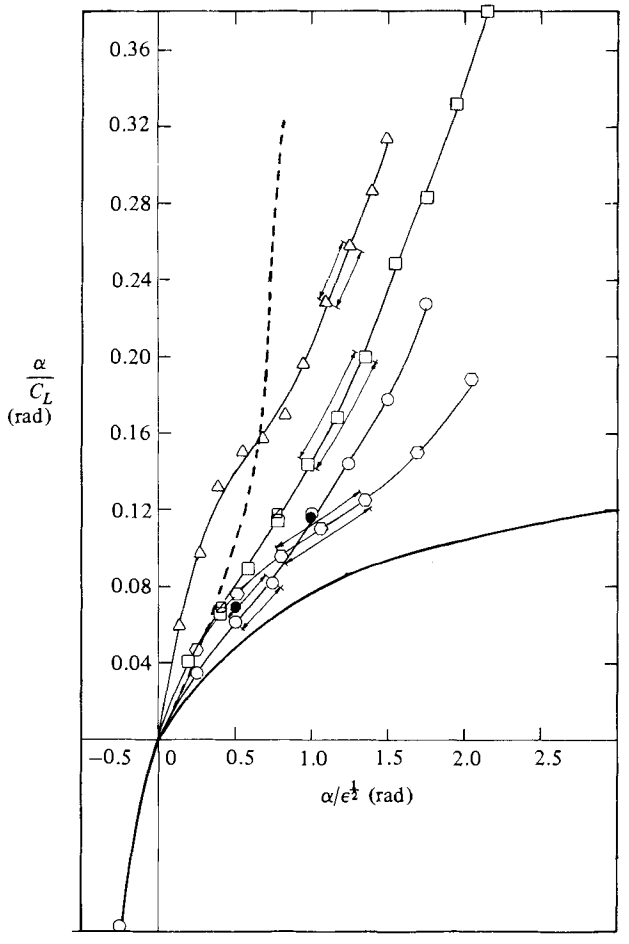

FIGURE 5. Lift coefficient. Theory: ——, conventional, Kutta condition at trailing-edge; – – – –, modified, Kutta condition at leading-edge. Experiment: ⬡, $\epsilon = 0.017$; ○, 0.03; □, 0.05; △, 0.10. Open symbols: thin supports, $Re = 1.2 \times 10^5$. Solid symbols: thick supports, $Re = 1.2 \times 10^5$, thin supports, $Re = 0.7 \times 10^5$, diagonal line through symbols. ⟺ indicates range of ideal incidence.

which results in a decrease of C_L with camber, and this is contrary to trend predicted by Nielsen (1963).

The values of tension coefficient C_T and the centre of lift are shown in figures 6 and 7, and exhibit the same trends. For the two smaller values of ϵ the results are consistent with one another at low $\alpha/\epsilon^{\frac{1}{2}}$ and show the best agreement with theory.

The membrane angles θ_L, θ_T, the maximum camber y_{MC} and its position x_{MC} (figures 8, 9 and 10 respectively), all of which are geometric parameters dependent on the shape of the membrane, are quite well predicted by the Nielsen theory and are clearly not a particularly sensitive test of its accuracy. The discrepancies in membrane angle near $\alpha = 0°$ do not show up on the θ/α plot in figure 8.

A contributory reason for the failure of the theory might be the linearization of the inviscid problem. Vanden-Broeck (1982) has solved the more complicated nonlinear problem. He presents a limited number of predictions which indicate that the effect of nonlinearity at small $\alpha/\epsilon^{\frac{1}{2}}$ is to *increase* C_T (his figure 8), which moves the predictions somewhat further from the experimental results. It is therefore improbable that nonlinear effects are important in resolving the present discrepancies.

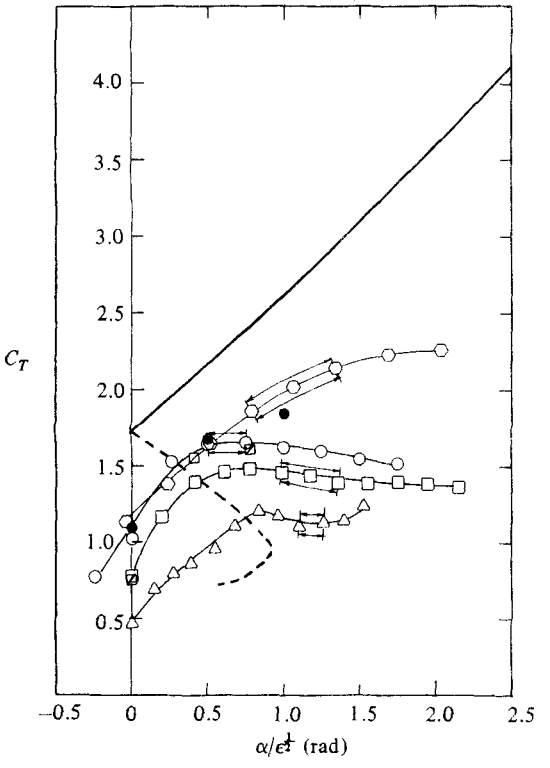

FIGURE 6

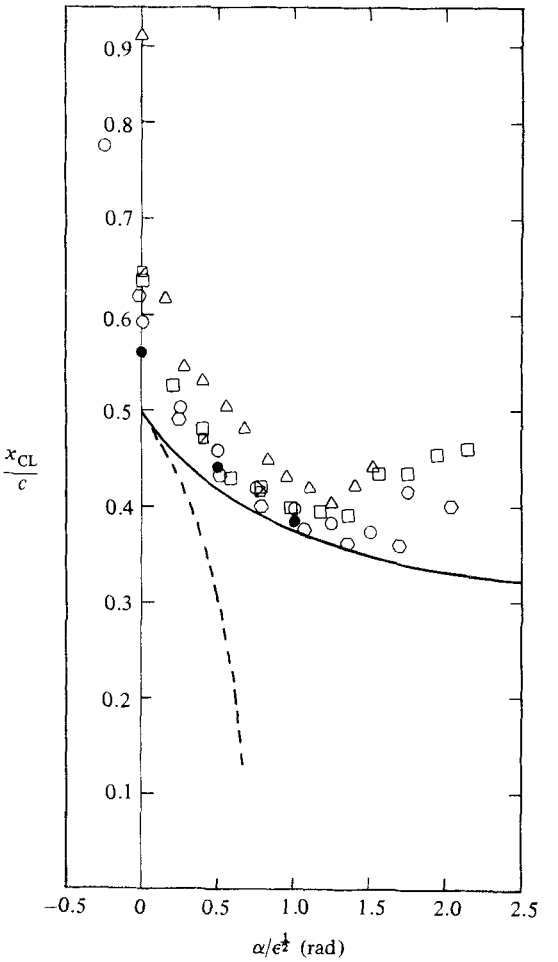

FIGURE 7

FIGURE 6. Tension coefficients; legend as in figure 5.

FIGURE 7. Centre of pressure; legend as in figure 5.

The basic cause of the discrepancies is the neglect of viscous effects, which become dominant when the flow separates at the leading edge. The first experimental indication of this effect was that the total measured forces on the leading- and trailing-edge supports were always very nearly equal, being slightly *larger* at the leading edge by an amount consistent with skin friction on both sides of the sail. Thus, as expected, the leading-edge suction force S, which would contribute to produce a smaller force on the leading edge for $\alpha \neq 0°$, is absent because the flow separates there.

In order to investigate the discrepancies the flow was examined visually. Small models with $\epsilon = 0.03$ and 0.08 were tested at $Re = 7 \times 10^3$ in a smoke tunnel. At $\alpha = 0°$ the smoke showed a leading-edge separation bubble over the 'lower' surface in both cases. For $\epsilon = 0.03$ the ideal incidence was $\alpha = 5°$, and there was some indication of separation near the trailing edge (figure 11). At $\alpha = 10°$ a separation bubble formed on the upper surface (figure 12), and at $\alpha = 15°$ the flow was completely separated. For $\epsilon = 0.08$ the ideal incidence was closer to 15°, and the trailing-edge separation was more pronounced. The loss of circulation associated with the thick, or even separated, boundary layer near the trailing edge at $\alpha = 0°$ causes the leading-edge

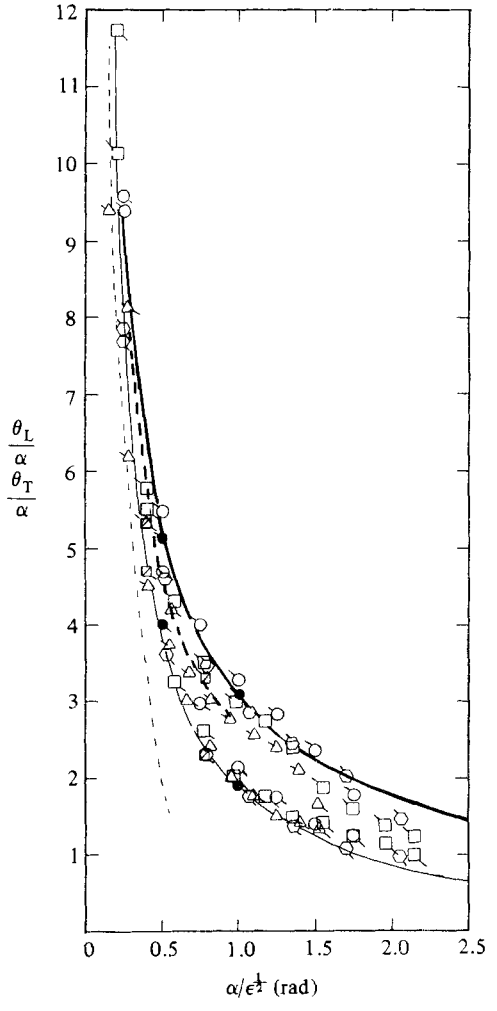

FIGURE 8

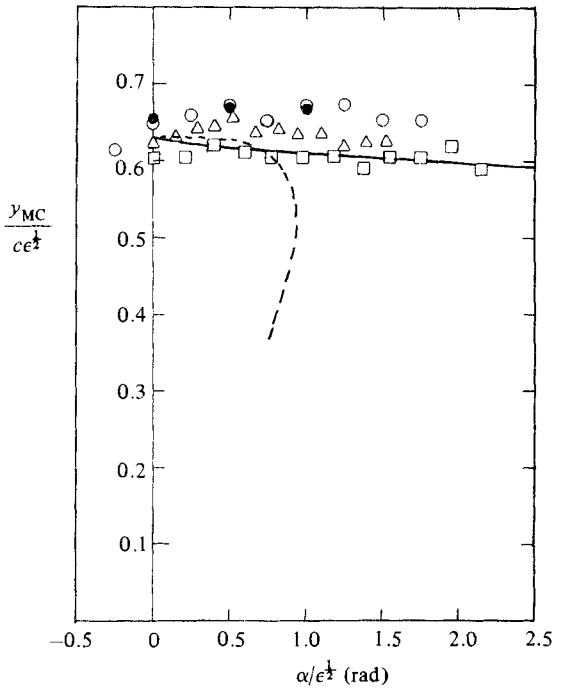

FIGURE 9

FIGURE 8. Leading- and trailing-edge membrane angles. Experiment: symbols as in figure 5. θ_L: ——, conventional theory; – – – –, modified theory; experiment with upper flags, e.g. ♉. θ_T: ——, conventional theory; –·–·–·–, modified theory; experiment with lower flags, e.g. ♌.

FIGURE 9. Camber ratio; legend as in figure 5.

stagnation point to move onto the upper surface, and leads to leading-edge separation over the lower surface and an S-shaped membrane. The photograph for $\epsilon = 0.08$ illustrates the effect particularly well (figure 13).

The regions of separation and reattachment were also measured on the main models at $Re = 1.2 \times 10^5$ using tufts attached to the models and wire-held single tufts in the case of the model with $\epsilon = 0.017$. The results are presented in figures 14 (*a–d*). They broadly agree with the smoke tunnel observations. At small α increasing ϵ produces a larger separation bubble on the lower surface and leads to separation of the flow from the upper surface near the trailing edge. A leading-edge separation bubble appears on the upper surface at higher α as ϵ is increased, and this eventually melds with the trailing-edge separation until the flow completely separates from the upper surface. With increasing α at fixed ϵ the lower-surface separation bubble disappears

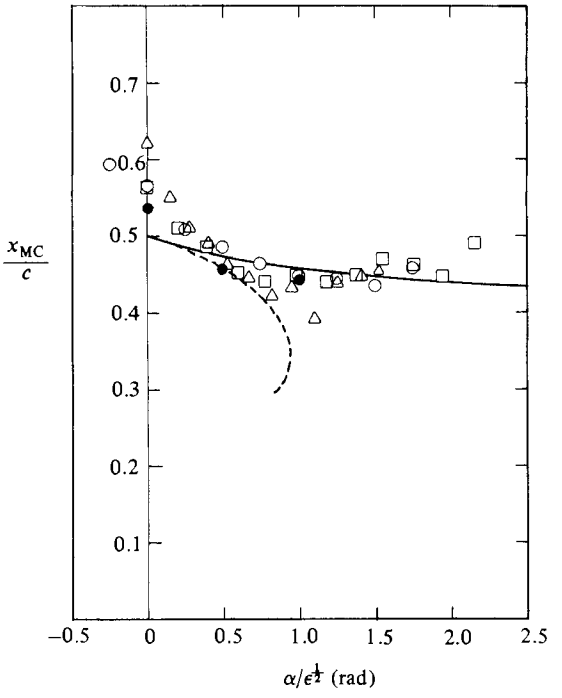

FIGURE 10. Position of maximum camber; legend as in figure 5.

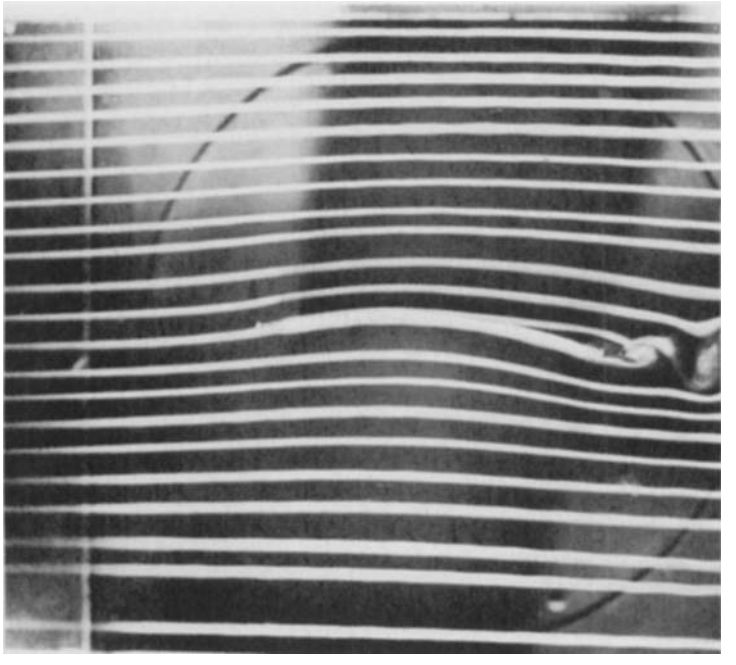

FIGURE 11. Smoke-tunnel photographs; flow from left to right; $Re = 7 \times 10^3$, $\epsilon = 0.03$, $\alpha = 5°$.

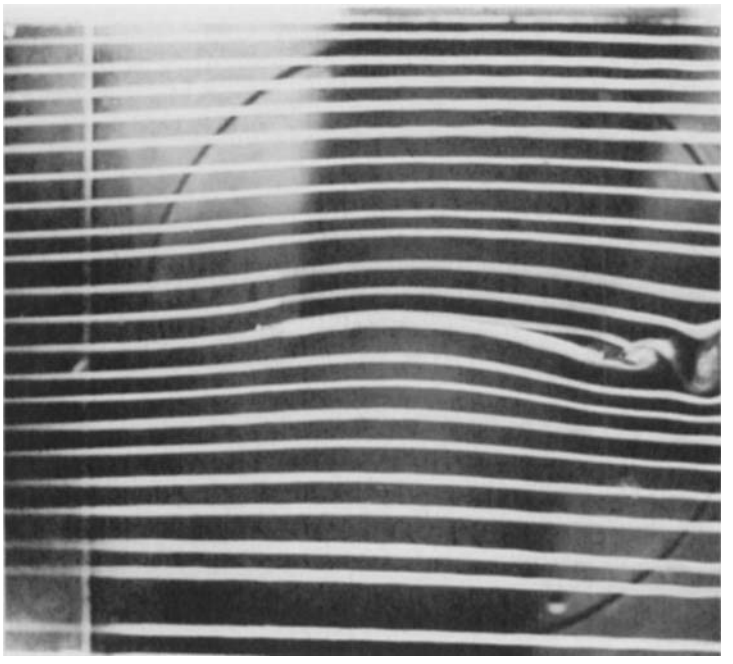

FIGURE 12. Smoke-tunnel photographs; flow from left to right; $Re = 7 \times 10^3$, $\epsilon = 0.03$, $\alpha = 10°$.

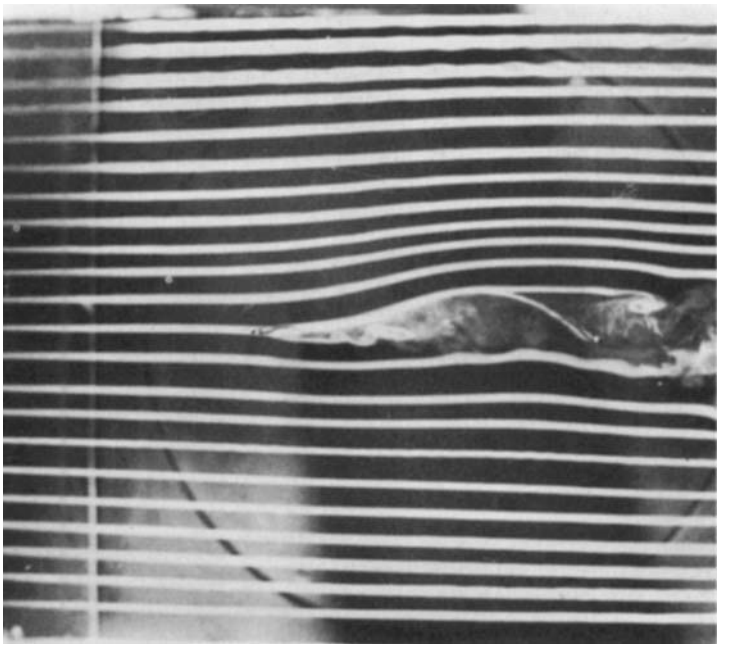

FIGURE 13. Smoke-tunnel photographs; flow from left to right; $Re = 7 \times 10^3$, $\epsilon = 0.08$, $\alpha = 0°$.

at the optimum incidence, and then a leading-edge separation bubble appears on the upper surface. For larger ϵ these effects occur at higher α.

In the case of $\epsilon = 0.017$ the supporting wedges dictated that there were always very small separation bubbles on both sides of the sail near the leading edge, as can be seen in figure 14 (*a*). The existence of equal bubbles of very small and minimum length, 0.09 *c*, was therefore chosen as the criterion for determining what would have been the range of ideal incidence if the wedges were vanishingly small in this case.

The present results are compared in table 1. The nominal camber ratio is that corresponding to a circular arc. Despite the large difference in Reynolds number and the approximate nature of the measurements, the results are in surprisingly good agreement. Although the stalling incidence is not too well defined, nevertheless it appears to occur at an incidence well below the values for which the flow completely separates from the upper surface.

For each value of ϵ there is a small range of sail incidence which is experimentally ideal in the sense that there is negligible separation at the leading edge. These ranges, which are between 2° and 5° in extent, are identified in figures 5 and 6. None of them embraces the theoretical value $\alpha = 0°$, and this has been attributed to the reduction of conventional circulation due to boundary-layer effects near the trailing edge. The modified theory in §2.2 in which the Kutta condition is applied at the leading edge instead of the trailing edge might therefore be expected to indicate how the measured results near the ideal incidence would deviate from the conventional theory in §2.1. In figures 5 and 6 it is seen that the values of α/C_L and C_T do lie between the two theories. In the modified theory the sail is S-shaped, whereas it is wholly concave in practice near the ideal incidence. Thus the remaining parameters in figures 7–10 which are very sensitive to membrane angle at the trailing edge are not well predicted by the modified theory.

At low incidence a sail exhibits a flapping instability at the leading edge which is known as luffing. The effect is usually attributed to bistable instability at $\alpha = 0°$ (Thwaites 1961; Nielsen 1963; Irvine 1979). In the linear inviscid theory the idea is that sail shape is symmetrical fore and aft at $\alpha = 0°$ and the Kutta condition is satisfied at the trailing edge. The sail is therefore just as likely to set itself on one side of the chord line as the other, and is thus in a bistable condition. The present observations indicate luffing incidences which are slightly negative. Specifically luffing occurred at $\alpha = -2\frac{1}{2}°$ for $\epsilon = 0.03$, $-1\frac{1}{2}°$ for $\epsilon = 0.05$ and $-1°$ for $\epsilon = 0.10$. At these incidences the sail luffed and eventually flipped over to the other side, giving an effectively positive incidence (wind flow now approaching the concave side of the sail) and a stable condition with lift in the opposite direction. The sail shape at luffing is, however, very different from theory. At $\alpha = 0°$, the failure of the Kutta condition due to boundary layer build-up and even separation near the trailing-edge places the leading-edge stagnation point on the upper side of the sail, resulting in a sail shape that is slightly reflexed (figure 13). It is therefore reminiscent of the theoretical shapes at negative incidence. This condition appears to be only just stable. Luffing finally occurs as the incidence is reduced to negative values and the stagnation point moves rearward on the upper surface.

Newman (1982) has examined the dynamic stability of a membrane with slightly different velocities on each side.† It was concluded that a sail would become unstable when

$$C_T < \frac{2\sigma/\rho c}{\pi\sigma/\rho\lambda + 1},$$

† *Note added in proof.* This solution was obtained for a travelling wave with complex frequency and real wavenumber.

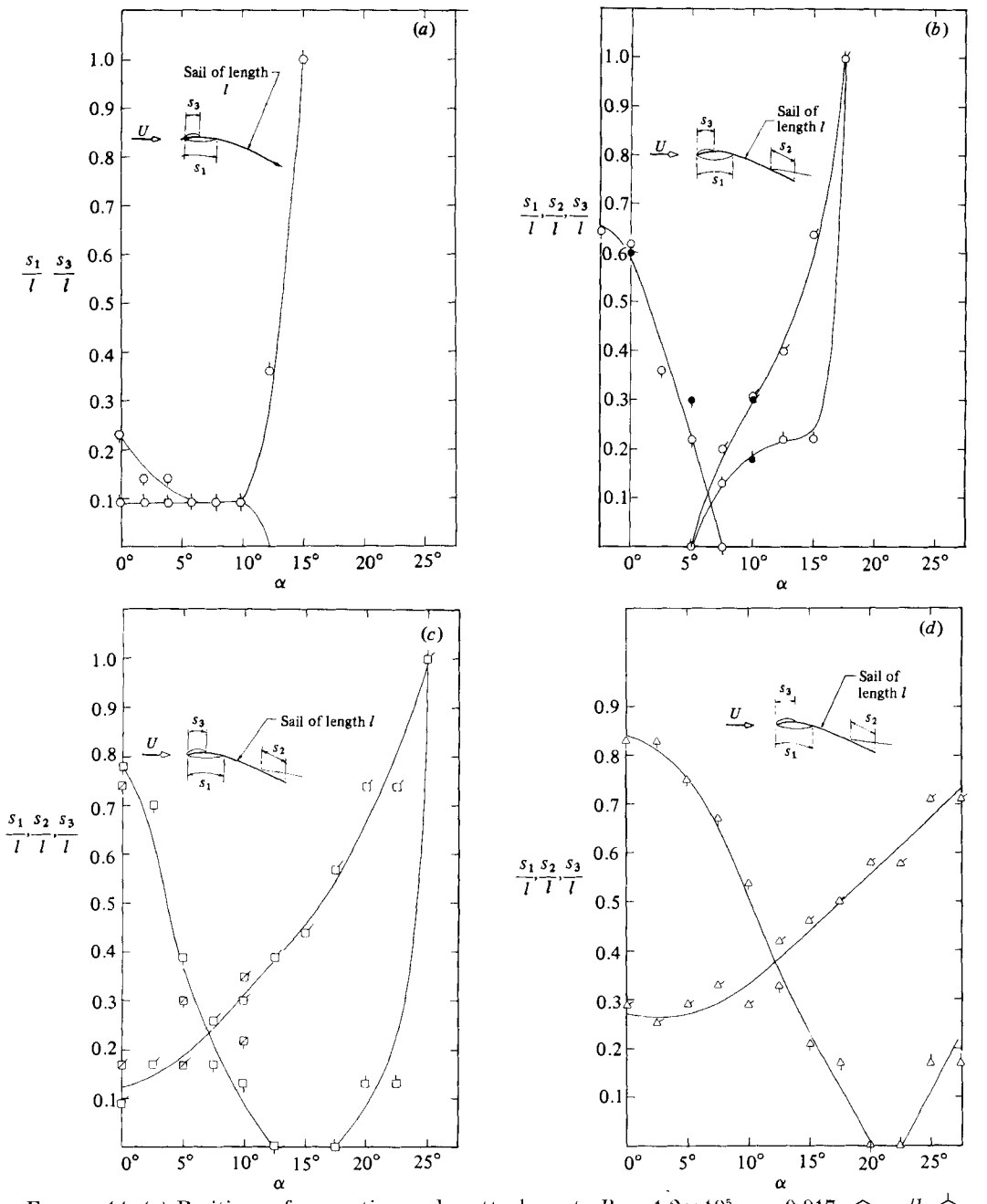

FIGURE 14. (*a*) Positions of separation and reattachment; $Re = 1.2 \times 10^5$, $\epsilon = 0.017$: ⬡, s_1/l; ⬡, s_3/l; wedge supports. (*b*) $\epsilon = 0.03$: ⚲, s_1/l; ⚲, s_2/l; ⚲, s_3/l; open symbols: thin supports; solid symbols: thick supports. (*c*) $\epsilon = 0.05$: ⊓, s_1/l; ⊓, s_2/l; ⊓, s_3/l; open symbols: $Re = 1.2 \times 10^5$; diagonal line through symbols: $Re = 0.7 \times 10^5$. (*d*) $\epsilon = 0.10$: ⏃, s_1/l; ⏃, s_2/l; ⏃, s_3/l.

where σ is the mass per unit area of the membrane and λ is the wavelength of the unstable oscillation. For the present experiments $\sigma/\rho c = 0.41$. The wavelength for a standing wave lies between 0 and $2c$. Thus instability occurs with the longest wavelength when $C_T < 0.5$. With this value figure 6 suggests that luffing would occur at about $-3\frac{1}{2}°$, and at $-2°$ and $0°$ for ϵ respectively equal to 0.03, 0.05 and 0.10. These values compare fairly well with the measured values of $-2\frac{1}{2}°$, $-1\frac{1}{2}°$ and $-1°$.

Re	ϵ	Observed ideal α	Complete separation α	Stall α at $C_{L\max}$	Nominal camber ratio $(\frac{3}{8}\epsilon)^{\frac{1}{2}}$
1.2×10^5	0.017	$6°$–$9\frac{1}{2}°$	15°	12°	0.077
Main models	0.03	$5°$–$7\frac{1}{2}°$	17°	12°	0.106
	0.05	$12\frac{1}{2}°$–$17\frac{1}{2}°$	24°	15°	0.137
	0.10	$20°$–$22\frac{1}{2}°$	40° extrapolated	17°	0.194
7×10^3	0.03	5°	15°	—	0.106
Smoke-tunnel models	0.08	15°	25°	—	0.173

TABLE 1. Comparison of the experimental results for the smoke-tunnel models and the main models

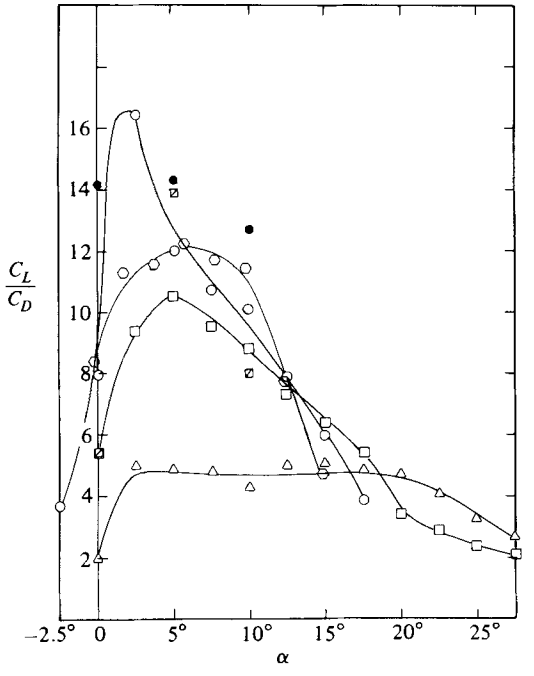

FIGURE 15. Lift-to-drag ratio; legend as in figure 5.

The measured drag of the present sails is presented in terms of lift-to-drag ratio in figure 15. In §2.3 it is shown that the lift divided by the leading-edge suction force in inviscid flow is

$$\frac{C_L}{C_S} = \frac{2}{\theta_T - \theta_L + 2\alpha}. \tag{10}$$

Owing to separation at the sharp leading edge, the drag D is at least as large as the lost suction force S, and the above equation therefore provides an upper limit to the lift-to-drag ratio. When the measured values of θ_T and θ_L in figure 8 are inserted into (10) at the values of α corresponding to the maximum values of C_L/C_D shown in figure 15, $C_L/C_S = 23$ for $\epsilon = 0.017$, 18 for $\epsilon = 0.03$, 16.5 for $\epsilon = 0.05$, and 6 for $\epsilon = 0.10$. These values are seen to be convincing upper limits to the maximum values in figure 15.

Rows	Investigation	Reynolds number	Camber ratio	C_L at $\alpha = 0°$	C_L maximum value	C_D at $\alpha = 0°$	C_D at $C_{L\max}$
(i)	Planar sail of $(l-c)/c = 0.017$, from present study	1.2×10^5	0.08	0.43	1.43 at $\alpha = 12\frac{1}{2}°$	0.05	0.18
	Thin cambered plate with maximum camber at 0.4 c, from Schmitz (1942)	1.7×10^5	0.058	0.45	1.12 at $\alpha = 8°$	0.03	0.09
(ii)	Streamlined membrane of $(l-c)/c = 0.03$, from present study	1.2×10^5	0.11	0.75	1.50 at $\alpha = 12\frac{1}{2}°$	0.09	0.19
	Circular arc with end-plates (aspect ratio not given), from Wallis' results in Chapleo (1968)	3.1×10^5	0.10	0.90	1.7 at $\alpha = 13°$ (C_D is not given at $\alpha = 13°$)	0.04	0.05 at $\alpha = 9\frac{1}{2}°$
(iii)	Streamlined membrane of $(l-c)/c = 0.05$, from present study	1.2×10^5	0.14	0.65	1.55 at $\alpha = 16°$	0.12	0.26
	Two-dimensional sails, from Chapleo (1968)	1.1×10^5	0.13	0.8	1.6 at $\alpha = 16°$	0.07	0.38
	Circular arc with aspect ratio corrected to ∞ from 5, from Eiffel's results in Chapleo (1968)	1.2×10^5	0.14	0.8	1.5 at $\alpha = 15°$	0.08	0.25
(iv)	Streamlined membrane of $(l-c)/c = 0.10$, from present study	1.2×10^5	0.20	0.36	1.55 at $\alpha = 18°$	0.16	0.33
	Two-dimensional sails, from Chapleo (1968)	1.2×10^5	0.2	0.7	1.8 at $\alpha = 16°$	0.15	0.4
				0.8	2.2 at $\alpha = 13°$	0.12	0.35
		1.1×10^5	0.21	0.8	2.2 at $\alpha = 19°$	0.12	0.42
				0.7	1.8 at $\alpha = 24°$	0.12	0.5
		1.1×10^5	0.25	0.4	1.7 at $\alpha = 20°$	0.22	0.42

TABLE 2. Lift and drag measurements of sails and circular arcs

The results for C_L and C_D at two angles of incidence ($\alpha = 0°$ and α at maximum C_L) are compared with previous results for sails and rigid cambered plates in table 2. As far as possible, comparable Reynolds numbers and camber ratios have been selected. The present results for the planar sail with camber ratios 0.08–0.14 ($\epsilon = 0.017$–0.05) show satisfactory agreement (see rows (i)–(iii) of table 2) with the previous measurements, and the detailed differences are no doubt due to dissimilar shape and camber. The present values of C_L for camber ratio 0.2 ($\epsilon = 0.10$) are significantly lower than those of Chapleo (1968) (row (iv) of table 2). However, Chapleo's results may be unreliable: certainly his values of camber are uncertain and his values of $C_{L\max}$ seem to be unusually high. The measurements described by Nielsen are for higher Reynolds numbers between 6 and 8×10^5, which are close to full-scale values. The lift-curve slope of the present experiments is nonlinear, and the average slopes for $\epsilon = 0.05$, and possibly 0.03, exceed the theoretical values, owing no doubt, to the changes in separation bubble size and hence effective camber as α is increased. By comparison, Nielsen states that the lift-curve slope is nonlinear and the average value exceeds the theoretical value when $\epsilon > 0.06$. In the present

investigation the centre of pressure in figure 7 is behind the theoretical position for very small α and tends to agree with the theory for values of $\alpha/\epsilon^{\frac{1}{2}} \approx 1$ and $\epsilon < 0.05$. Nielsen asserts that agreement is good for all non-zero values of α and for $\epsilon < 0.06$. The present experiments are therefore only broadly in agreement with Nielsen's.

It was not possible to increase the Reynolds number of the present measurements, because of limitations on model size and permissible deflection of the supports. The Reynolds number was therefore reduced as much as was practicable and a few results for $Re = 0.7 \times 10^5$ and $\epsilon = 0.05$ are shown in figures 5–10, 14(*c*) and 15. The lift (figure 5), camber (figure 7) and separation and reattachment positions (figure 14*c*) were not significantly changed by this small reduction of Reynolds number. However, the lift-to-drag ratio, tension and the membrane angles were affected, particularly at $\alpha = 10°$. These particular discrepancies are attributed to flaccidity of the model at the lower tunnel speed, for which the dynamic pressure was insufficient to fully tauten the fabric.

The Reynolds number of the present measurements is 5–10 times smaller than typical full-scale values. The effect of such an increase of Reynolds number would be to reduce boundary-layer thickness near the trailing edge, and this would lead to ideal incidences closer to the theoretical value of 0°. However, leading-edge separation bubbles would still be present, and conventional theory would be significantly in error. Schmitz's (1942) results for a rigid curve plate give an indication of the magnitude of the effect. When the Reynolds number was increased from 4×10^4 to 4×10^5 there was a 15% increase of lift.

5. Conclusions

1. The present measurements disagree with linearized inviscid theory for two-dimensional impervious sails, particularly when the excess-length ratio exceeds 0.03. The lift and tension coefficients are significantly less than the theoretical values. The discrepancies are not attributed to the linearity of the theory, but are due to boundary-layer separation bubbles at the leading edge and boundary-layer effects near the trailing edge.

2. Near the ideal incidence for which there is smooth flow at the leading edge the values of lift and tension lie between the conventional linearized theory and a modified theory in which the Kutta condition is applied at the leading edge rather than the trailing edge.

3. The maximum lift-to-drag ratio was 16.5 and was obtained at $\alpha = 2°$ on a membrane with $\epsilon = 0.03$. The corresponding ratio of lift to theoretical suction force was 18.

4. Luffing is a dynamic rather than a bistable instability. It therefore depends on the surface density of the membrane σ and occurs when the tension coefficient is less than $2/(\frac{1}{2}\pi + \rho c/\sigma)$.

This work was supported by NSERC Grant A7096 awarded to B. G. Newman and a Canadian Commonwealth Scholarship awarded to H. T. Low.

REFERENCES

BARAKAT, R. 1968 Incompressible flow around porous two-dimensional sails and wings. *J. Maths & Phys.* **47**, 327–349.

CHAPLEO, A. Q. 1968 A review of two-dimensional sails. *Univ. Southampton SUYR Rep.* 23.

IRVINE, H. M. 1979 A note on luffing in sails. *Proc. R. Soc. Lond.* A **365**, 345–347.

JACKSON, P. S. 1983 A simple model for elastic two dimensional sails. *AIAA J.* **21**, 153–155.

LOW, H. T. 1982 Planar two-dimensional flow past membranes. Ph.D. thesis, McGill University.

MARCHAJ, C. A. 1979 *Aero-Hydrodynamics of Sailing.* Dodd Mead.

MILGRAM, J. H. 1971 Sail force coefficients for systematic rig variations. *Soc. Nav. Arch. and Mar. Engng T. & R. Rep.* R-10.

MILGRAM, J. H. 1972 Sailing vessels and sails. *Ann. Rev. of Fluid Mech.* **4**, 397–430.

MURAI, H. & MARUYAMA, S. 1980 Theoretical investigation of the aerodynamics of double membrane sailwing aerofoil sections. *J. Aircraft* **17**, 294–299.

MURAI, H. & MARUYAMA, S. 1982 Theoretical investigation of sailwing airfoils taking account of elasticities. *J. Aircraft* **19**, 385–389.

NEWMAN, B. G. 1982 The aerodynamics of flexible membranes. *Proc. Indian Acad. Sci.* **5**, 107–129.

NEWMAN, B. G. & LOW, H. T. 1981 Two-dimensional flow at right angles to a flexible membrane. *Aero. Q.* **32**, 243–269.

NIELSEN, J. N. 1963 Theory of flexible aerodynamic surfaces. *Trans. ASME* E*: J. Appl. Mech.* **30**, 435–442.

ORMISTON, R. A. 1971 Theoretical and experimental aerodynamics of the sailwing. *J. Aircraft* **8**, 77–81.

PANKHURST, R. C. & HOLDER, D. W. 1952 Wind tunnel technique. Pitman.

ROBERT, J. & NEWMAN, B. G. 1979 Lift and drag of a sail aerofoil. *Wind Engng* **3**, 1–22.

ROBINSON, A. & LAURMANN, J. A. 1956 *Wing Theory.* Cambridge University Press.

SCHMITZ, F. W. 1942 Aerodynamik des Flugmodells. C. J. E. Volckmann, Berlin.

SWEENEY, T. E. 1961 Exploratory sailwing research at Princeton. *Aero Engng Rep.* 578.

THWAITES, B. 1960 *Incompressible Aerodynamics.* Oxford University Press.

THWAITES, B. 1961 Aerodynamic theory of sails. *Proc. R. Soc. Lond.* A **261**, 402–422.

VANDEN-BROECK, J. M. 1982 Nonlinear two-dimensional sail theory. *Phys. Fluids* **25**, 402–423.

VOELZ, VAN K. 1950 Profil und Auftrieb eines Segels. *Z. angew. Math. Mech.* **30**, 301–317.

WYGNANSKI, I. & GARTSHORE, I. S. 1963 General description and calibration of the McGill 17 in. × 30 in. blower cascade wind tunnel. *Mech. Engng Res. Lab. Tech. Note* 63–7, *McGill University.*